PRELIMINARY AND INCOMPLETE

How have pandemics ended? Modelling recurrent outbreak risk following the main waves

Max Schroeder[1], Spyridon Lazarakis[2], Rebecca Mancy[1]✉, Konstantinos Angelopoulos[1, 3]

Abstract

Empirical evidence from municipal public health records and national data reveals that multiple outbreaks followed the main waves of the 1847-48 and 1890-91 influenza pandemics in England and Wales, as well as the 1918-19 influenza pandemic in the US and in eight major cities in the UK. To characterise the latent recurrent outbreak risk, we model the stochastic process of mortality rates following the main pandemic waves as a sequence of bounded Pareto distributions such that mortality risk and the associated probability of large outbreaks declines exponentially over time. We fit this model to the post-pandemic data and, with striking consistency across pandemics and geographical areas, we find elevated recurrent outbreak risk that persists for nearly two decades.

Keywords: Post-pandemic outbreaks; Outbreak risk dynamics; Influenza; Archives

[1] University of Glasgow, Glasgow, UK, [2] Lancaster University, Lancaster, UK, [3] CESifo, Munich, Germany
✉ email: Rebecca.Mancy@glasgow.ac.uk

Main text

Introduction

Existing research has suggested the possibility of recurrent outbreaks following the main waves of pandemics (Anderson & May, 1992; Giannitsarou, Kissler, & Toxvaerd, 2021; Kissler, Tedijanto, Goldstein, Grad, & Lipsitch, 2020; Lavine, Bjornstad, & Antia, 2021; McKie, 2021; Oxford, 2000; Phillips, 2021). We examine outbreaks during the post-pandemic period that followed historical pandemics of respiratory tract infections. Specifically, we compile municipal public health records and use national data to investigate the empirical time series of disease outbreaks following the main waves of the 1847-48 and 1890-91 influenza pandemics in England and Wales, as well as the 1918-19 influenza pandemic in the US and in eight major UK cities. Visual inspection of the time series of outbreaks reveals that across locations and scales, the main pandemic waves were followed by multiple recurrent outbreaks in the following decades. Such recurrent outbreaks during the post-pandemic period and the implied uncertainty regarding their occurrence are important because they can have severe implications for health and socioeconomic outcomes (Angelopoulos, Lazarakis, Mancy, & Schroeder, 2021; Mamelund & Dimka, 2021; Marmot, 2020; Marmot & Allen, 2020; Stantcheva, 2021).

A formal characterisation of the persistence of mortality risk that follows the main pandemic waves and the timeframe over which it fades are essential to help researchers, policymakers and practitioners from a broad range of backgrounds to respond appropriately during a post-pandemic period. However, statistical models using historical data to characterise the time evolution of this risk are currently missing from the literature. We model the stochastic process of mortality rates following the main pandemic waves as a sequence of bounded Pareto distributions such that the inverse of the tail index of these distributions decays exponentially. By fitting the model to the historical post-pandemic municipal and national data, we find that it predicts persistently elevated recurrent outbreak risk for nearly two decades before more rapid convergence to pre-pandemic levels.

Empirical observations of post-pandemic mortality rates

To motivate our statistical modelling, we use data from three historically important pandemics to shed light on the time evolution of influenza mortality after the main waves. Our dataset consists of historical mortality rates from influenza for eight large municipalities across the UK between 1895 and 1956, alongside published data for England and Wales between 1838 and 1917, and national level data for the US between 1900 and 1956. This period captures three major pandemics in 1847-48, 1890-91 and 1918-19 (Hill, Tildesley, & House, 2017). The start dates reflect data availability, and the end dates are chosen to focus the analysis on the post-pandemic period until a new pandemic.

We compiled data from a range of sources. We transcribed city-level data from the Medical Officer of Health (MOH) reports, annual administrative documents covering a range of public health-related issues at the municipal level. The first reports begin in the mid-19th century, and coverage extends to most municipalities in the UK until the early 1970s. The reports used here can be viewed on the Wellcome Trust Collection website, with tables available in the form of images of the relevant pages (Wellcome Trust, 2021). We used the annual reports for Belfast, Birmingham, Cardiff, Glasgow,

London (London County Council MOH reports), Liverpool, Manchester and Sheffield to compile influenza mortality data between 1895 and 1956. Annual mortality rates by cause of death are generally presented in tables within each report or its appendices (or could be computed as the ratio of the number of deaths to the population size). Despite changes over time to the taxonomy of causes of death, influenza was reported consistently in the MOH reports across the period under consideration. During the war years, 1914-1919 and 1939-1945, some reports are missing, or the data provided is incomplete. Where possible, we recovered the missing information by assessing statistics for these years from later reports. Data for the US were compiled from annual tables covering the period 1900-1960 contained within the Vital Statistics Rates Reports of the National Center for Health Statistics. Data for England and Wales between 1838 and 1917 were taken from Langford (2002), who compiled mortality rates from different sources.

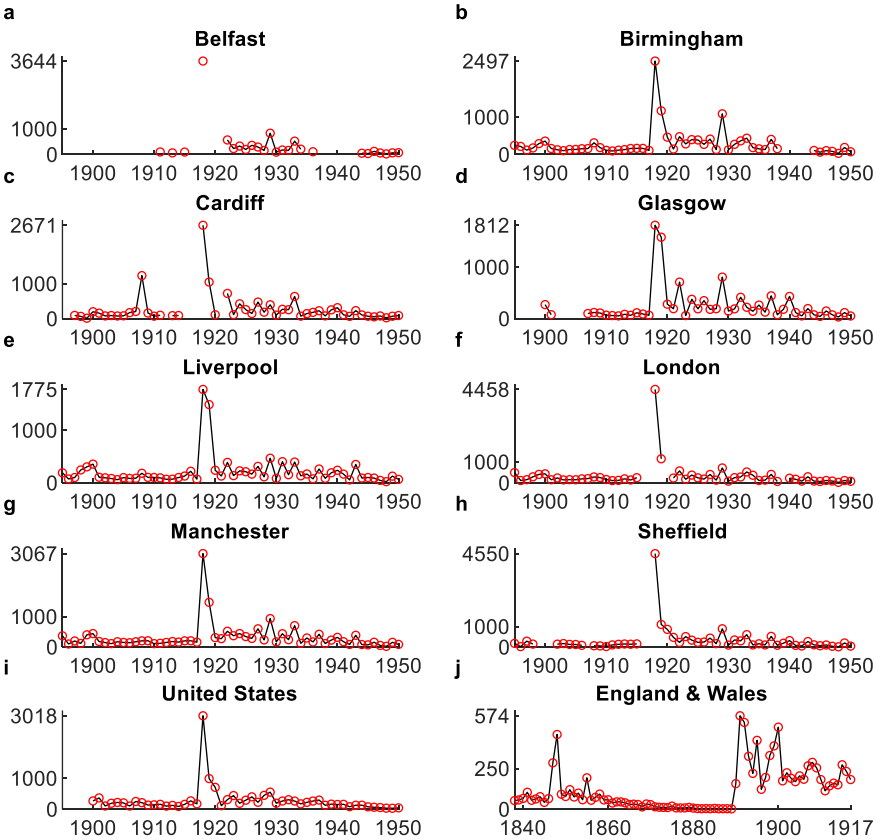

Figure 1. Annual mortality rate from influenza. Mortality rate in deaths per million population. The upper y-axis tick indicates the maximum mortality rate for each data series. Data for UK cities are taken from Medical Officer for Health reports. Data for the US are taken from Lindner and Grove (1943) *and Grove and Hetzel* (1968)*. Data for England & Wales are taken from Langford* (2002)*, Table 5.*

Figure 1 shows the time series of annual mortality rates from influenza for the different geographies. The key insight from the time series is that influenza mortality rates remain elevated and more variable for a long period after pandemics. Focusing on the eight British municipalities (a)-(h), although the most striking feature is the massive increase in mortality in 1918 and 1919 due to the main pandemic waves, we also observe spikes of high mortality in the series post-1920 that continue for an extended period. The same pattern emerges in the US (i) with respect to the 1918-19 influenza pandemic, while a similar pattern of disease outbreaks is observed following the 1847-8 and the 1890-91 influenza pandemics in England and Wales (j). We note that there is some ambiguity about the dates of some pandemics, and, for the

period prior to around 1900 (relevant for our England and Wales analysis), whether some spikes in the data constitute pandemics or recurrent outbreaks of earlier strains. For example, some scholars consider the spike in 1900 as a (symptomatically mild) pandemic, but more recent sources consider it an outbreak of the 1890-91 strain; some scholars treat the spike in 1857, which we treat as a recurrent outbreak because of its relatively lower impact, as a pandemic (see, e.g. Hill et al., 2017 for a discussion).

Contemporary expert evaluations by the Medical Officer for London corroborate the findings from the data shown in Figure 1. We examined available London County Council MOH reports between 1920 and 1957 to identify discussions of elevated influenza rates in each year. In each report, we performed a search for the phrase *influenza*. Because public health officials were particularly attentive to influenza after the 1918-19 pandemic, virtually every annual report contains at least some discussion of the disease. The language of the reports clarifies whether a certain year is considered to have had a notable outbreak of influenza, while some reports further include retrospective reflections on past influenza outbreaks. These reports identify 1922, 1924, 1927, 1929, 1933 and 1937 as years of heightened mortality from influenza, in line with the time series we constructed.

Modelling post-pandemic mortality dynamics

We aim to formally characterise the latent outbreak risk underpinning the post-pandemic outbreaks observed in the data. To do so, we model the dynamic evolution of annual mortality rates after the main pandemic waves as outcomes drawn from a sequence of bounded Pareto distributions. We assume that the inverse of the tail index of the bounded Pareto distributions decays exponentially after the main waves of the pandemic such that mortality risk and the probability of large outbreaks declines over time.

Mathematically, we denote the mortality rate in year t by d_t, for $t = 0,1,2, \dots, N$, where the time period refers to $(1920, 1921, \dots, 1956)$ for the eight cities in the UK and the US with reference the 1918-19 pandemic, to $(1849, 1850, \dots, 1890)$ for England and Wales with reference to the 1847-48 pandemic, and to $(1892, 1893, \dots, 1917)$ for England and Wales with reference to the 1890-91 pandemic. In each year, mortality rates are drawn from

$$d_t \sim PD_t(d_l, d_u, \alpha_t), \qquad (1)$$

where PD_t denotes the bounded Pareto distribution in period t, $\alpha_t > 0$ is the time-varying Pareto tail index, and $d_l > 0$ and $d_u > d_l$ are, respectively, lower and upper bounds. Defining $\eta_t = {}^{1}/_{\alpha_t}$, we assume the time process

$$\eta_t = e^{\eta_0} e^{-\lambda t}, \qquad (2)$$

where $\lambda > 0$ determines the rate at which the inverse tail index decays over time, while η_0 sets the initial level of the probabilities. The two main modelling assumptions incorporated in (1) – (2) are: firstly, that, in every year, the mortality rates follow a bounded Pareto distribution; and secondly, that mortality risk, as determined by the inverse of the Pareto tail coefficient, declines following the main waves. We discuss these below (see also SI for further discussion and robustness analysis).

The size of outbreaks in a given year has been shown to be highly over-dispersed and is well modelled by a fat-tailed distribution such as a bounded Pareto (Cirillo &

Taleb, 2020). The bounded Pareto also offers both flexibility and tractability in the dynamic model in (1) – (2). In particular, a model of the dynamics of mortality risk after the main pandemic waves needs to be sufficiently flexible to capture risk both during the period of relatively high mortality soon after the main waves and that of lower mortality a few decades later. Therefore, the underlying distribution in any given year should be able to simultaneously capture this pattern, achieved via a fat tail, while the mass of the distribution is at the lower end of mortality. When the tail becomes less important, the distribution converges to a very high concentration toward the lower bound, implying lower mortality rates. The bounded Pareto distribution has these characteristics: the most likely outcomes remain near the lower bound despite a fat tail. In addition, it has the advantage of tractability because conditional on the bounds, a transition in the tail probabilities is captured by changes in a single parameter. Further discussion of these points and results based on alternative modelling choices, including a one-parameter Weibull distribution, can be found in SI.

The decline in mortality risk over time, captured in the model specification by (2), is motivated by the empirical observations shown in Figure 1. These observations imply that influenza mortality risk starts from a relatively high level, eventually converging to background mortality (i.e. a level comparable with that immediately prior to the relevant pandemic, as well as several decades later). Under the assumption that risk decreases over time, the model in (1)-(2) describes the level of risk and its rate of decline as a function of the parameters η_0 and λ, which determine the sequence $(\alpha_t)_{t=0}^{N}$. Although (2) constrains the inverse of the tail index α_t to decay exponentially, it does not impose such a restriction on probabilities associated with the tails. Indeed, although the probabilities of different mortality rates are a monotonic function of the tail index and thus decrease over time, the inverse of a convex function does not have a predetermined convexity, and $\lambda > 0$ implies that the rate of decline of the probabilities can take on a range of forms. This feature is evident in our results.

To fit the model to the data, we take as given the main pandemic waves and fit to the data over the subsequent years. During subsequent recurrent outbreaks, mortality is lower, so we set the upper bound of mortality rates to the maximum mortality rate of the main waves. Similarly, we set the lower bound of mortality to background influenza mortality, defined here as the lowest mortality experienced after the relevant pandemic and prior to the following pandemic (i.e. the lowest mortality observed in the relevant sample). As we discuss in more detail in SI, the main results are robust to modelling instead d_l and d_u as theoretical upper and lower bounds of mortality rates. However, by exploiting information pertinent to the pandemic and geographic unit in parameterising d_l and d_u, any common pattern that is observed can be considered emergent rather than imposed. Moreover, by letting the bounds differ between geographical units, we allow for differences in the mortality of the main pandemic waves, and in latent socioeconomic and public health conditions that can impact mortality associated with these bounds.

Model fitting

We fit our model of post-pandemic mortality rate dynamics to the data for each geographical unit conditional on its own experience of the pandemic and background mortality, as summarised by the parameters d_l and d_u. Conditional on d_l and d_u, the

two parameters η_0 and λ then determine the dynamics of mortality and disease outbreak risk by controlling the level and time evolution of probabilities of outcomes associated with the tail of the Pareto distributions.

We obtain λ and η_0 by maximising the likelihood function:

$$L(\lambda, \eta_0) = \prod_{t=0}^{N} \frac{\left(e^{\eta_0 e^{-\lambda t}}\right)^{-1} (d_l)^{\left(e^{\eta_0 e^{-\lambda t}}\right)^{-1}} (\bar{d}_t)^{-\left(e^{\eta_0 e^{-\lambda t}}\right)^{-1}-1}}{1-\left(\frac{d_l}{d_u}\right)^{\left(e^{\eta_0 e^{-\lambda t}}\right)^{-1}}}, \qquad (3)$$

given a sample of mortality rates $\left(\bar{d}_t\right)_{t=0}^{N}$ (see SI for more details, which also reports parameter estimates for all geographies). We examine the small sample properties of the maximum likelihood estimator by undertaking a Monte Carlo analysis. Treating the estimated parameters for each geography as the "true" parameters, we generate 10,000 samples of data and estimate the parameters from these. Each Monte Carlo sample is a sequence of mortality rates of the same length as the post-1918 data. The contour plots in Figure 2 provide a visualisation of the joint probability density of the estimated parameters from these simulations under the assumption that the true data generating processes are those estimated for London, Glasgow, Liverpool (a-c), as well as the US and England and Wales after the two relevant pandemics (d-f). As can be seen, the joint distributions are unimodal, and in all cases the median is effectively the same as the parameter value under the true data generating process. In SI, we show that similar results are obtained for all geographies for which we have estimated (1)-(2).

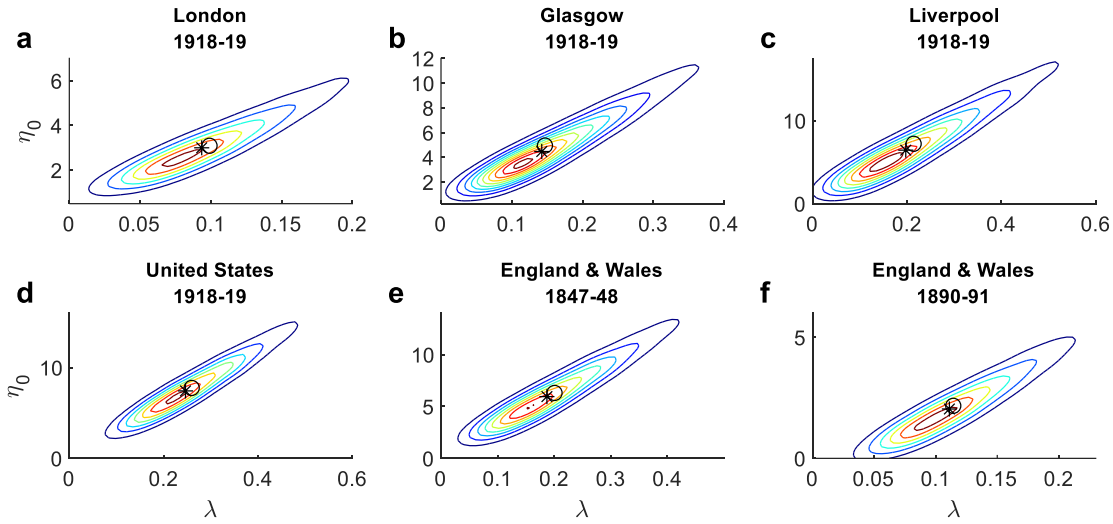

Figure 2: Monte Carlo analysis showing the correspondence between true parameter values (stars) and medians (circles) of 10,000 Monte Carlo simulations. Contour lines represent the probability densities of combinations of η_0 and λ obtained from smoothed parameter kernel densities from the Monte Carlo simulations.

Figure 3 shows the time series of data points overlaid on model predictions of outcomes based on the model fitted to the same geographical units as in Figure 2 (see SI for remaining geographies). In particular, we plot the median, interquartile range and 80% interval of the estimated bounded Pareto distribution for each year. As can be seen, most observations lie within the interquartile, with observed outcomes outside these bounds reflecting indeed "rare events".

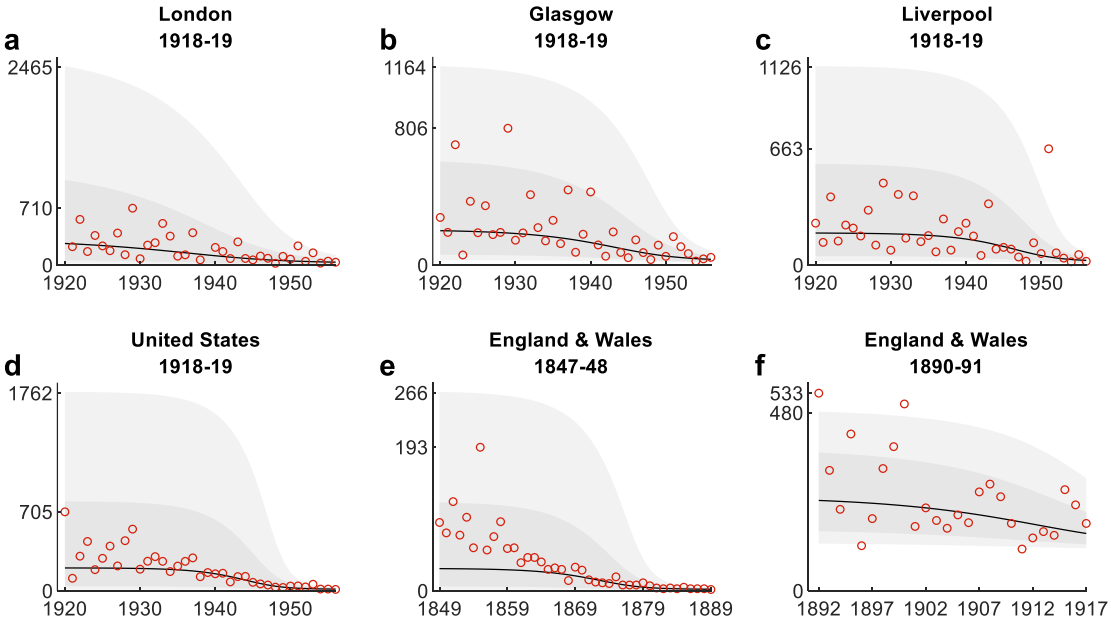

Figure 3. Model predicted influenza mortality rates following pandemics for selected geographies. Interquartile range (dark shading) and 80% prediction interval (light shading), with observed mortality rates overplotted in red. Ticks on y-axis show the upper values of the 80% prediction interval and maximum observed value in the data. Data sources shown in Figure 1.

Recurrent outbreak risk dynamics

Having obtained the time series of distributions of mortality rates in the decades that followed the main pandemic waves, we can calculate the probability of mortality above a specified rate in each year. By defining a disease outbreak as mortality above a threshold, we can compute the time series of outbreak risk.

Figure 4 shows the post-pandemic disease outbreak probabilities for different thresholds. In particular, for the 1918-19 pandemic, we define two disease outbreak thresholds at 500 and 1000 deaths per million. The 500-per-million threshold represents substantially higher mortality than any mortality rate between 1900 and 1918 (i.e., after the 1890-91 pandemic effects had died out). It also corresponds to mortality observed during the main waves of the 1890-91 pandemic and subsequent outbreaks. For the period after 1920, this threshold identifies as outbreaks the same years as those described as having exceptionally high influenza mortality in the MOH reports for London. The 1000-per-million threshold approximates that of the severe 1929 outbreak. More generally, this threshold identifies particularly large disease outbreaks that were *possible* given the dynamic process for mortality risk, even if unrealised *ex post*. Similarly, for the 1847-48 and the 1890-91 pandemics in England and Wales, we show post-pandemic disease outbreak probabilities for different thresholds.

Two central results stand out in Figure 4. First, the probability of a disease outbreak remains high for about two decades after the main pandemic waves, and unlike the exponential decline of the tail parameter, declines only very slowly during this period. Second, the pattern of the time evolution is similar across all geographical units, despite considerable differences in the scale of the main waves and background influenza mortality.

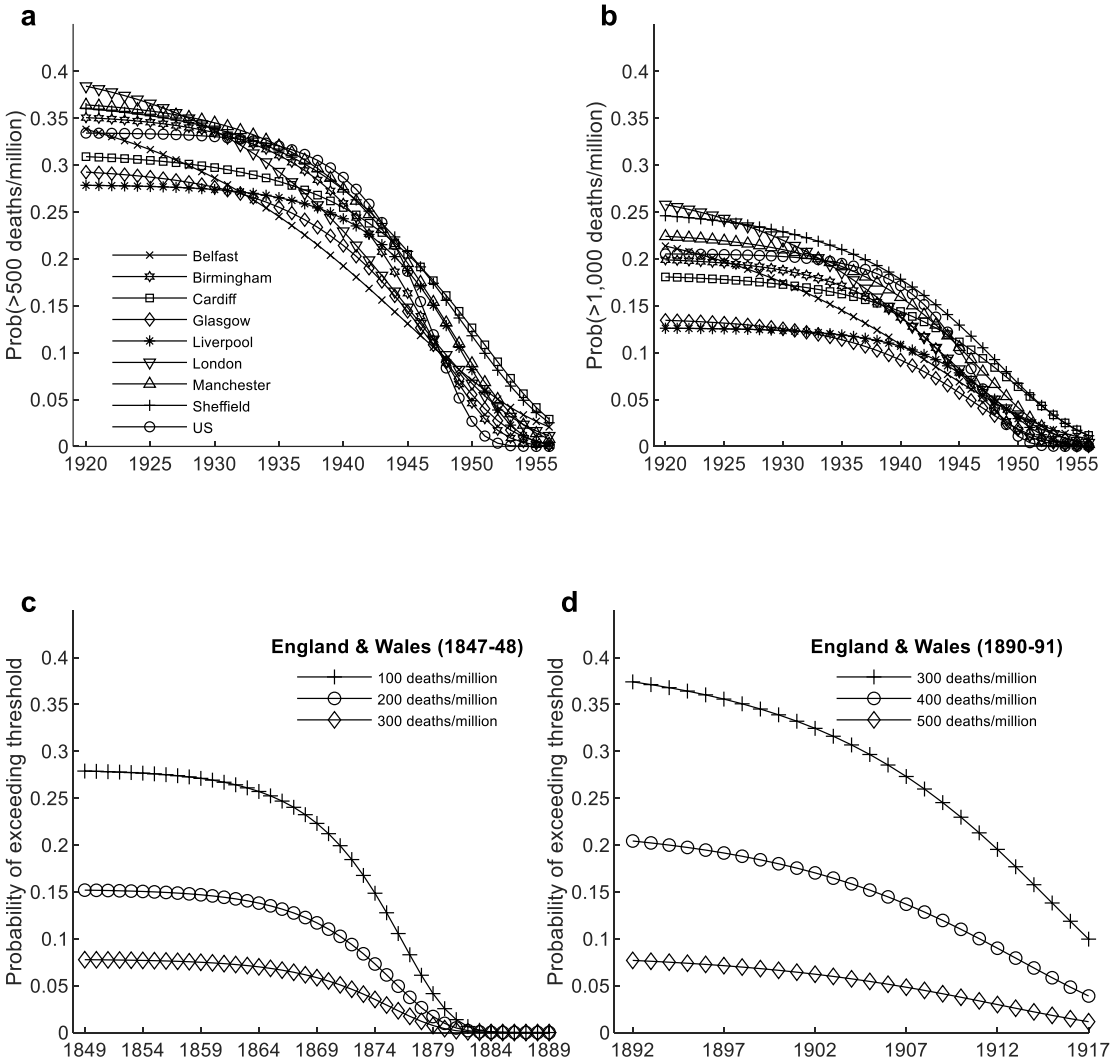

Figure 4. Outbreak risk following the 1918-19, 1847-48 and 1890-91 pandemics. (a)-(b) Outbreak probabilities computed from models fitted to each city and the US, for thresholds of (a) 500 deaths per million and (b) 1000 per million. (c)-(d) Outbreak probabilities computed from the model fitted to data for England and Wales following the 1847-48 pandemic and 1890-91, for different thresholds.

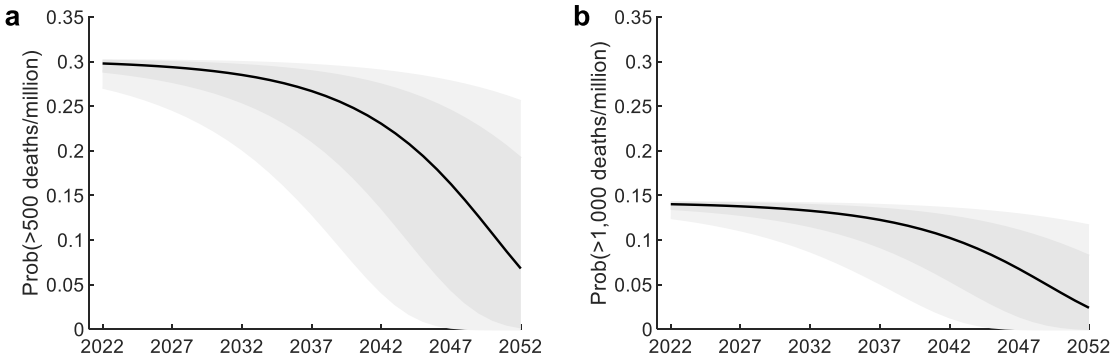

Figure 5. Simulated outbreak probabilities for COVID-19, showing median (solid black line), interquartile range (dark shading) and 80% prediction interval (light shading), based on 1m random draws. Outbreak probabilities are computed from model parameterisations that are drawn from a distribution of η_0 and λ implied by the models fitted to historical data. The upper bound on future mortality ($d_u = 1858$) is set equal to COVID-19 mortality in the UK in 2020 and the lower bound ($d_l = 24$) to reflect mortality in the non-pandemic state, approximated by background influenza mortality pre-2020 (data sources in SI).

Application to COVID-19: Lessons from the past for the present

To uncover the underlying epidemiological risk before the effect of modern means of intervention we use the historical mortality risk estimates to simulate mortality dynamics after the main waves of COVID-19. The generality of the main qualitative characteristics of the dynamic risk patterns in Figure 3, across geographical units with different experience of the main wave and background mortality, suggests that the model in (1) – (2) can be used for counterfactual analysis. The quantitative predictions are dependent on the bounds of the Pareto distributions, as well as the specific sequence $(\alpha_t)_{t=0}^{N}$ used, or equivalently on the underlying parameter values for η_0 and λ. Regarding the bounds of the Pareto distributions, these are determined by the experience of the pandemic to which the model predictions apply.

To simulate underlying mortality risk after COVID-19, we set the upper bound on future mortality to be determined by COVID-19 mortality in the UK in 2020 and the lower bound to reflect mortality in the non-pandemic state in the coming decades, which we approximate by background influenza mortality pre-2020. We use the range of values of η_0 and λ across the different geographical units from our historical analysis to approximate the joint distribution of possible parameter values; this approach thus assumes that, beyond the upper and lower bounds taken from the COVID-19 data, we assume no additional effect of modern means of intervention. Then, for one million draws from this joint distribution, we compute the disease outbreak probabilities and relevant percentiles.

Figure 5 shows model-predicted probabilities of disease outbreaks in the form of mortality rates exceeding 500 and 1000 per million from our counterfactual analysis after the main waves of COVID-19. These results demonstrate elevated disease outbreak risk for two decades. In 90% of model-predicted dynamic paths, the probability of outbreaks exceeding 500 deaths per million, which is 20 times higher than seasonal influenza, is above 20% for a decade and remains above 10% for nearly two decades. Regarding outbreaks closer in scale to mortality during the first main wave, in 90% of model-predicted dynamic paths, the probability of outbreaks exceeding 1000 deaths per million is above 10% for a decade. The results suggest the importance of continued prevention, monitoring and preparedness efforts, even well after the main waves.

Concluding remarks

Our central finding is that mortality risk remains elevated for a prolonged period after the main pandemic waves. The similarity of the pattern of disease outbreak dynamics across geographic units with different socioeconomic characteristics and three historical pandemics highlights the generality of this result. Our analysis contributes to the literature in two main ways. Firstly, we provide direct empirical evidence of medium-run persistence of outbreak risk after the main waves of previous pandemics, at multiple spatial scales and in multiple locations. Secondly, we develop a parsimonious statistical model to uncover latent outbreak risk after the main waves of a pandemic and demonstrate how it can be used, even with relatively sparse data, to reveal persistence of risk for around two decades.

Our findings contribute to understanding mortality risk in the period that follows pandemics. Understanding post-pandemic mortality risk is important because outbreak risk generates health and economic uncertainty which has significant and

unequal consequences for socioeconomic outcomes across the population. Specifically, because disease outbreaks imply a deterioration in health outcomes that is not symmetric across the population (Mamelund & Dimka, 2021; Marmot, 2020; Marmot & Allen, 2020; Quinn & Kumar, 2014), a period of increased disease outbreak risk implies the possibility of repeated negative impacts on health inequality. Moreover, outbreak risk generates social, political and economic uncertainty, stemming from possible impacts of the disease itself and of containment measures on economic activity. Increased aggregate-level uncertainty further impacts economic decision-making, income inequality and economic fluctuations, either directly or via increased idiosyncratic risk (Angelopoulos, Lazarakis, & Malley, 2020, 2021; Bloom, 2009; Bloom, Floetotto, Jaimovich, Saporta-Eksten, & Terry, 2018; Heathcote, Storesletten, & Violante, 2010).

The potentially high persistence of disease outbreak risk for many years after a pandemic highlights the value of scientific and medical developments and policy preparedness. Indeed, medicine, public health, technology, and better-informed and prepared policy intervention offer the opportunity in the modern world to confront post-pandemic recurrent outbreak risk better than a century ago. The overall message from our analysis is that ongoing prevention strategies and policy preparedness to mitigate outbreaks are likely to be required, even well after the main pandemic waves.

References

Anderson, R. M., & May, R. M. (1992). *Infectious Diseases of Humans: Dynamics and Control (Oxford Science Publications)*. Retrieved from http://www.amazon.co.uk/Infectious-Diseases-Humans-Dynamics-Publications/dp/019854040X

Angelopoulos, K., Lazarakis, S., & Malley, J. (2020). The distributional implications of asymmetric income dynamics. *European Economic Review*, *128*, 103502. https://doi.org/10.1016/J.EUROECOREV.2020.103502

Angelopoulos, K., Lazarakis, S., & Malley, J. (2021). Cyclical labour income risk in Great Britain. *Journal of Applied Econometrics*. https://doi.org/10.1002/JAE.2860

Angelopoulos, K., Lazarakis, S., Mancy, R., & Schroeder, M. (2021). *Pandemic-induced wealth and health inequality and risk exposure* (No. 9474).

Bloom, N. (2009). The Impact of Uncertainty Shocks. *Econometrica*, *77*(3), 623–685. https://doi.org/10.3982/ecta6248

Bloom, N., Floetotto, M., Jaimovich, N., Saporta-Eksten, I., & Terry, S. J. (2018). Really Uncertain Business Cycles. *Econometrica*, *86*(3), 1031–1065. https://doi.org/10.3982/ecta10927

Cirillo, P., & Taleb, N. N. (2020). Tail risk of contagious diseases. *Nature Physics*, *16*(6), 606–613. https://doi.org/10.1038/s41567-020-0921-x

Giannitsarou, C., Kissler, S., & Toxvaerd, F. (2021). Waning Immunity and the Second Wave: Some Projections for SARS-CoV-2. *American Economic Review: Insights*, *3*(3), 321–338. https://doi.org/10.1257/aeri.20200343

Grove, R. D., & Hetzel, A. M. (1968). *Vital statistics rates in the United States, 1940-1960* (Vol. 83). US Department of Health, Education, and Welfare, Public Health Service ….

Heathcote, J., Storesletten, K., & Violante, G. L. (2010). The macroeconomic implications of rising wage inequality in the United States. *J. Polit. Econ.*, *118*(4), 681–722. https://doi.org/10.1086/656632

Hill, E. M., Tildesley, M. J., & House, T. (2017). Evidence for history-dependence of influenza pandemic emergence. *Scientific Reports*, *7*(1), 43623. https://doi.org/10.1038/srep43623

Kissler, S. M., Tedijanto, C., Goldstein, E., Grad, Y. H., & Lipsitch, M. (2020). Projecting the transmission dynamics of SARS-CoV-2 through the postpandemic period. *Science*, *368*(6493), 860–868. https://doi.org/10.1126/science.abb5793

Langford, C. (2002). The age pattern of mortality in the 1918-19 influenza pandemic: an attempted explanation based on data for England and Wales. *Medical History*, *46*(1), 1–20. https://doi.org/10.1017/S002572730006871X

Lavine, J. S., Bjornstad, O. N., & Antia, R. (2021). Immunological characteristics govern the transition of COVID-19 to endemicity. *Science*, *371*(6530), 741–745. https://doi.org/10.1126/science.abe6522

Linder, F. E., & Grove, R. D. (1943). *Vital statistics rates in the United States, 1900-1940*. US Government Printing Office.

Mamelund, S.-E., & Dimka, J. (2021). Social inequalities in infectious diseases. *Scandinavian Journal of Public Health*, 140349482199722. https://doi.org/10.1177/1403494821997228

Marmot, M. (2020). Health equity in England: The Marmot review 10 years on. *The BMJ*, *368*, m693. https://doi.org/10.1136/bmj.m693

Marmot, M., & Allen, J. (2020). COVID-19: exposing and amplifying inequalities.

Journal of Epidemiology and Community Health, *74*(9), jech-2020-214720. https://doi.org/10.1136/jech-2020-214720

McKie, R. (2021, July 31). UK can expect thousands of Covid deaths every year, warn scientists | Coronavirus | The Guardian. Retrieved from the Guardian website: https://www.theguardian.com/world/2021/jul/31/uk-can-expect-thousands-of-covid-deaths-every-year-warn-scientists?CMP=Share_iOSApp_Other

Oxford, J. S. (2000). Infuenza A pandemics of the 20th century with special reference to 1918: virology, pathology and epidemiology. *Reviews in Medical Virology* , *10*(2), 119–133. https://doi.org/10.1002/(SICI)1099-1654(200003/04)10:2

Phillips, N. (2021). The coronavirus is here to stay - here's what that means. *Nature*, *590*(7846), 382–384. https://doi.org/10.1038/D41586-021-00396-2

Quinn, S. C., & Kumar, S. (2014). Health inequalities and infectious disease epidemics: A challenge for global health security. *Biosecurity and Bioterrorism*, *12*(5), 263–273. https://doi.org/10.1089/bsp.2014.0032

Stantcheva, S. (2021). Inequalities in the Times of a Pandemic. *Economic Policy*. Retrieved from https://www.economic-policy.org/wp-content/uploads/2021/04/9103_Inequalities-in-the-Times-of-a-Pandemic.pdf

Wellcome Trust. (2021, February 24). The Medical Officer of Health reports. Retrieved August 18, 2021, from https://wellcomelibrary.org/moh/about-the-reports/about-the-medical-officer-of-health-reports/

Conflicts of interest
The authors declare no conflicts of interest.

Data availability
The municipal level dataset generated during the current study are available on GitHub at https://github.com/maxschr90/Schroeder-et-al.-2021--How-long-do-pandemics-last-. Data for the US and for England and Wales are available from original publications, as described and referenced in the caption of Figure 1.

Code availability
Code is freely available on GitHub at https://github.com/maxschr90/Schroeder-et-al.-2021--How-long-do-pandemics-last-.

Prior versions
A previous versions of this paper is available at:
https://www.econstor.eu/bitstream/10419/249020/1/cesifo1_wp9475.pdf

Acknowledgements and funding
This project is supported by a grant that is funded by the Economic and Social Research Council (ESRC) as part of UK Research and Innovation's rapid response to COVID-19 (ES/V005898/1). The project also received support from the College of Social Sciences College Research Fund 2020/21, and from the Adam Smith Business School Student Internship Scheme, University of Glasgow. The project is supported by Glasgow City Archives, Glasgow Life. RM's contribution to this work was also supported by The Leckie Fellowship, the Medical Research Council [grant number MC_UU_00022/4] and the Chief Scientist Office [grant number SPHSU19].

Supplementary Information for

How have pandemics ended? Two decades of recurrent outbreak risk following the main waves.

Max Schroeder, Spyridon Lazarakis, Rebecca Mancy, Konstantinos Angelopoulos

Rebecca Mancy
Email: Rebecca.Mancy@glasgow.ac.uk

This PDF file includes:

Contents

Data sources

City-level data were compiled from Medical Officer of Health (MOH) reports. These reports were annual administrative documents covering a range of public health-related issues at the municipal level. The first reports begin in the mid-19th century, and coverage extends to most municipalities in the UK until the early 1970s. The reports used here have been made available online on the Wellcome Trust Collection website.[1] These have been partially digitised and are searchable by keyword, but quantitative data needed to be transcribed manually.

We collected influenza mortality data between 1895 and 1956 for eight large municipalities from across the UK: Belfast, Birmingham, Cardiff, Glasgow, London, Liverpool, Manchester and Sheffield. To do this, we searched relevant MOH reports for each municipality (for London, this is the London County Council MOH report). Generally, annual mortality rates by cause of death are presented in tables within the report or its appendices (or could be computed as the ratio of the number of deaths to the population size). Despite changes over time to the taxonomy of causes of death, *influenza* was reported consistently in the MOH reports throughout the decades. During the war years, 1914-1919 and 1939-1945, some reports are missing, or the data provided is incomplete. In these cases, we recovered the missing information by assessing statistics for these years from later reports, where possible. The dataset from the MOH reports underlying this research paper is available on GitHub at https://github.com/maxschr90/Schroeder-et-al.-2021--How-long-do-pandemics-last-.

Data for the US are taken from the Vital Statistics Rates Reports compiled by the National Center for Health Statistics. Specifically, we transcribe data from tables in the two special volumes[2,3] covering the period 1900-1960. Both volumes are available on the CDC's website.[4] Data for England and Wales between 1838 and 1917 are taken from Langford (2002, Table 5)[5], who compiles mortality rates from different sources.

To obtain COVID-19 mortality for the analysis in Figure 5, we combined the total number of UK COVID-19 deaths between 6th March 2020 and 6th March 2021 (124,654).[6] With mid-year population data from the ONS for 2020 (67,081,000).[7] This implies a mortality rate of 1,858 per million. Pre-2020 deaths from influenza are taken from the 2018-19 total mortality figures for England & Wales from the ONS[8] together with the mid-2018 population figures for England & Wales.[9]

Details of model of mortality risk dynamics

Details of fitting the model described in the main text

The model in equations (1) – (2) in the main text assumes that mortality rates after the main waves of the pandemic are the outcomes of a sequence of bounded Pareto distributions, where the inverse of the tail index of these distributions decays exponentially over time. The parameters $d_l > 0$ and $d_u > d_l$ scale the range of mortality rates that the model predicts. We fit the model to the data for each geographical unit and conditional on its own experience of the pandemic. Hence, we choose the bounds to reflect the realised range of mortality rates for the geographical unit over the period modelled. Conditional on d_l and d_u, the two parameters η_0 and λ then determine the dynamics of mortality and disease outbreak risk via controlling the level and time evolution of probabilities of outcomes associated with the tail of the Pareto distributions.

We obtain λ and η_0 by maximising the likelihood function:

$$L(\lambda, \eta_0) = \prod_{t=0}^{N} \frac{\left(e^{\eta_0 e^{-\lambda t}}\right)^{-1} (d_l)^{\left(e^{\eta_0 e^{-\lambda t}}\right)^{-1}} (\bar{d}_t)^{-\left(e^{\eta_0 e^{-\lambda t}}\right)^{-1}-1}}{1-\left(\frac{d_l}{d_u}\right)^{\left(e^{\eta_0 e^{-\lambda t}}\right)^{-1}}},$$

given a sample of mortality rates $\left(\bar{d}_t\right)_{t=0}^{N}$. To maximise the log likelihood function, we use MATLAB's fmincon routine, using a sequential quadratic programming algorithm. Derivatives are approximated by central numerical derivatives, and the relevant termination criteria are set to $1e^{-12}$. To account for potential nonconvexities and the presence of local maxima, we begin the maximisation from 1000 random seed values. Parameters are provided in Table *Table* .

Table A1: Model parameters. Maximum likelihood estimates of $\boldsymbol{\eta_0}$ and $\boldsymbol{\lambda}$ for the model specification described in the main text. Parameters $\boldsymbol{d_l}$ and $\boldsymbol{d_u}$ are the lower and upper bounds, respectively, of the mortality rate. The lower bound is the lowest mortality rate observed after the main waves and until the next pandemic, while the upper bound is the maximum observed during the main waves.

	λ	η_0	d_l	d_u
Cities				
Belfast	0.0739	2.4695	22	3644
Birmingham	0.1611	4.8565	27	2497
Cardiff	0.1336	4.9167	13	2671
Glasgow	0.1424	4.4664	24	1812
Liverpool	0.1973	6.4452	19	1775
London	0.0936	2.9999	23	4458
Manchester	0.1357	4.4422	23	3067
Sheffield	0.1169	4.2642	12	4550
US	0.2463	7.4299	14	3018
England & Wales 1847-48	0.1871	5.9514	2	459
England & Wales 1890-91	0.1111	2.0392	113	574

We examine the small sample properties of the maximum likelihood estimator by undertaking a Monte Carlo analysis. Treating the estimated parameters for each geography as the "true" parameters, we generate 10,000 samples of data of length 37, and estimate the parameters from these. The contour plots in Figure provide a visualisation of the joint probability density of the estimated parameters from these simulations under the assumption that the true data generating processes are those estimated for each city (for the national level data, see Figure 2 in the main text).

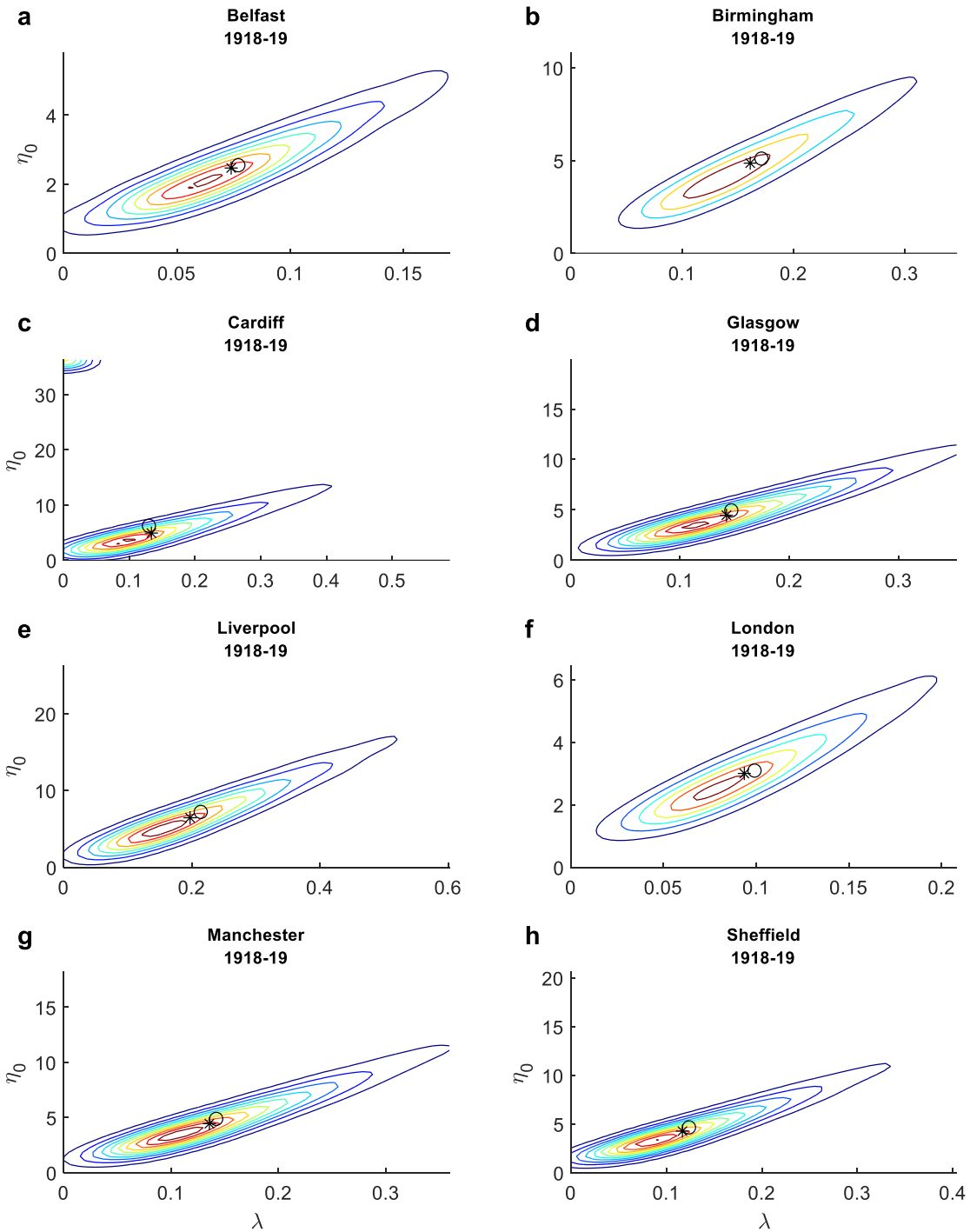

Figure A1. Monte Carlo analysis showing the correspondence between true parameter values (stars) and medians (circles) of 10,000 Monte Carlo simulations for cities. Contour lines represent the probability densities of combinations of $\boldsymbol{\eta_0}$ and $\boldsymbol{\lambda}$ obtained from smoothed parameter kernel densities from the Monte Carlo simulations.

Figure shows the time series of data points overlaid on model predictions of outcomes that are based on the model fitted to each city (the corresponding figures for the national level data are shown in Figure 3 in the main text). In particular, we plot the median, interquartile range and 80% interval of the estimated bounded Pareto distribution for each year.

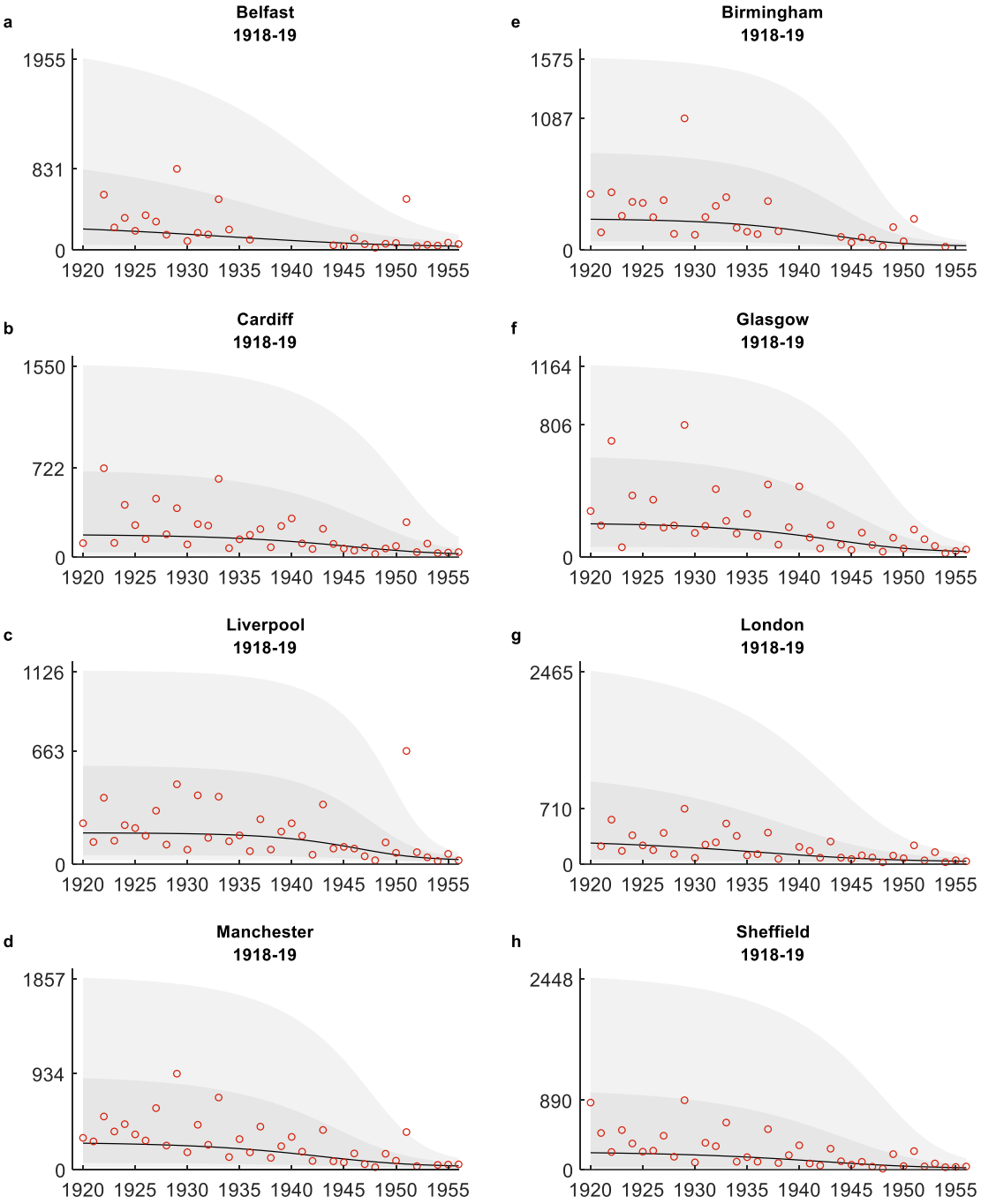

Figure A2. Model predicted influenza mortality rates following pandemics for cities. Median (solid line), interquartile range (dark shading) and 80% prediction interval (light shading), with observed mortality rates overplotted in red. Ticks on y-axis show the upper values of the 80% prediction interval and maximum observed value in the data. Data sources shown in Figure 1 in the main text.

Model with common mortality bounds across cities

We also examined a model with common mortality bounds across cities. The choice of the bounds, d_l and d_u, scales the range of mortality rates. The bounds used for the model used in the main text are shown in Table . The advantage of letting d_l and d_u be specific to the geographical unit studied is that we allow for differences in the experience of the pandemic and in conditions that influence background infectious disease mortality to have a bearing on risk dynamics. By allowing for such latent variation, our finding of a general pattern of mortality and disease outbreak risk dynamics is stronger.

Unsurprisingly, if we set d_l and d_u to be common across all cities, specifically to the lowest and highest mortality rate observed across them, the overall pattern is one where there is even greater similar across cities (relative to that shown in Figure 4 a-b).

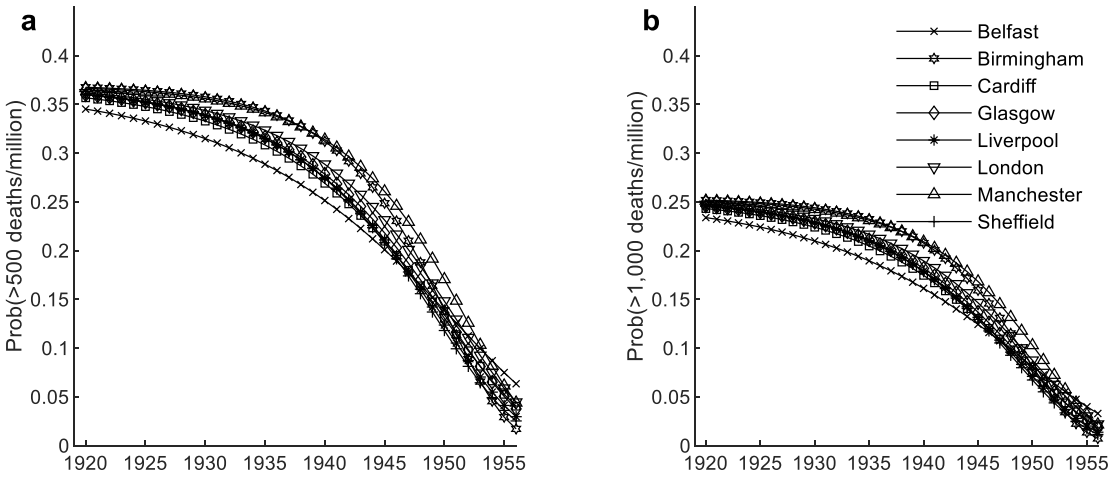

Figure A3: Outbreak risk following the 1918-19 pandemic (model with common bounds). Outbreak probabilities computed from models fitted to each city. Upper and lower bounds are common and set, respectively, to be the highest and lowest mortality rates within the sample of cities.

Model with theoretical mortality bounds

We also compared our main approach in which we specify the bounds of the Pareto distribution conditionally on the mortality range relevant to the geographical unit to a more agnostic approach of setting d_u and d_l to be determined by theoretical upper and lower bounds of mortality rates. Figure A3 reproduces Figure 4 under the agnostic modelling approach. As shown in Figure A3, the probability of a disease outbreak remained high until the 1940s, but the dynamic pattern is different from that in Figure 4 and implies increased and more persistent disease outbreak risk. Overall, agnostic modelling of d_l and d_u confirms high and persistent mortality risk after the main pandemic waves, as well as similarity across geographical units.

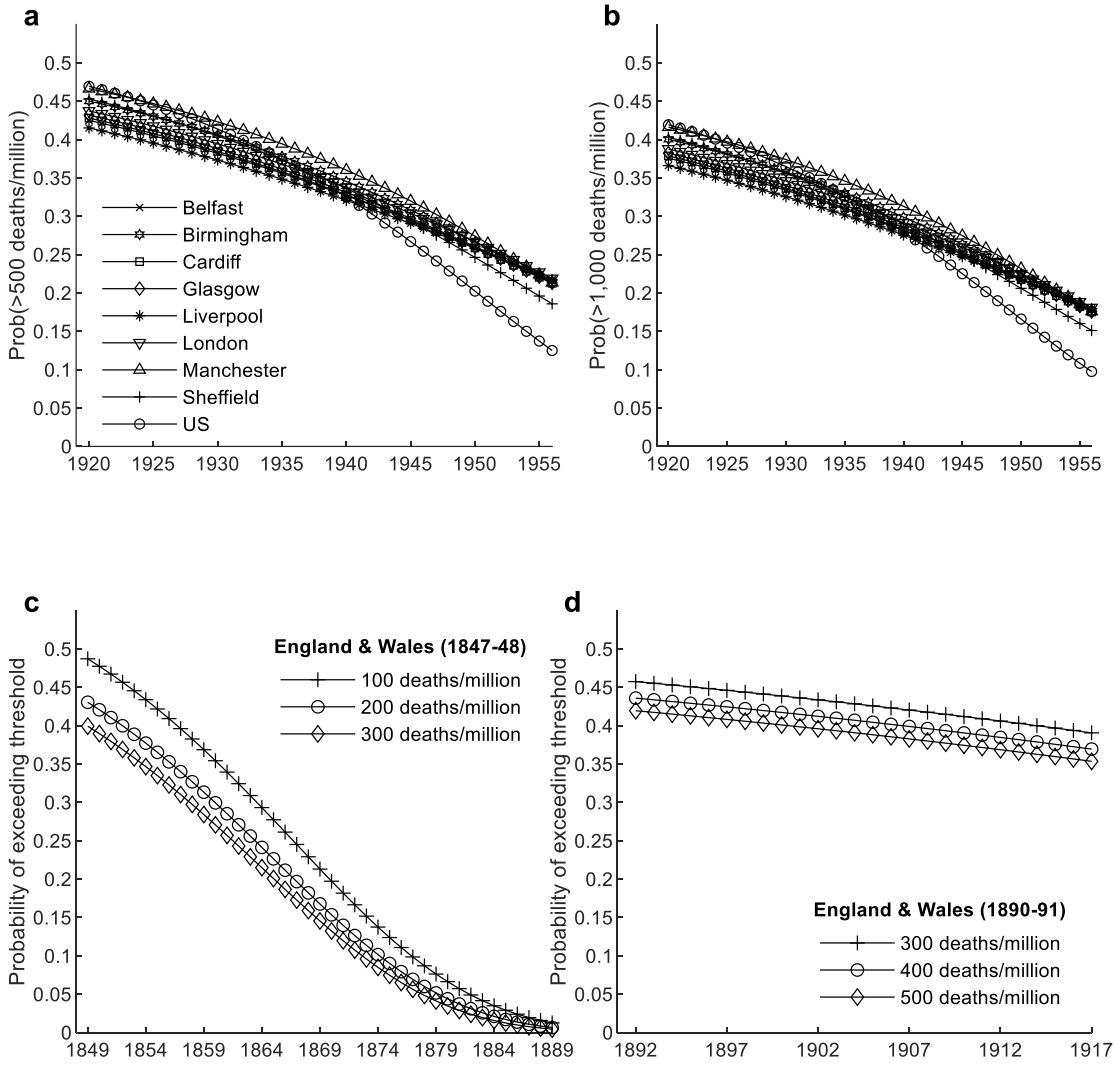

Figure A4: Outbreak risk following the relevant pandemic using the model with theoretical bounds, set to 1,000,000 (upper) and 1 (lower). (a-b) for the models fitted to the city data and the US following the 1918-19 pandemic, for thresholds of 500 and 1,000 per million; (c-d) for the models fitted to the England & Wales data following the 1847-48 pandemic (c) and the 1889-90 pandemic (d) for different thresholds.

Model with estimated mortality bounds

In our model fitting strategy in the main text, we calibrate d_l and d_u, exploiting out-of-sample information from the main pandemic waves to calibrate d_u. Technically, however, d_l and d_u can be estimated jointly with η_0 and λ using the time series following the main pandemic waves (i.e., without exploiting the information on the mortality effect of the main pandemic waves). In this case, equation (3) in the main text is maximised by choosing all four parameters, following the same optimisation methods as for the model in (1) – (2). Figure A4 reproduces Figure 4 under this methodology.

However, the model predictions in this case do not capture disease outbreak risk. In particular, although fitting the model in (1) – (2) by estimating all four parameters from the time series of data following the main pandemic waves may be useful for some applications (e.g. if the interest is in summarising historical experience), conceptually, this is no longer a model of mortality and disease outbreak *risk* dynamics, i.e. of the time evolution of the probability of disease outbreaks. Instead, d_l and d_u should, in this case, be interpreted as parameters chosen to maximise the fit of the process to the data, and thus are chosen by the optimisation routine to be, in effect, the maximum and minimum mortality observed between 1920 and 1956. In turn, this rules out the possibility of disease outbreaks that are higher than those observed *ex post*, even if theoretically they could have happened. An analysis of risk dynamics must account for the

possibility of higher mortality than that which was actually observed. Our modelling approach in the main text views bounds as *possible* even if unrealised mortality rates, given the experience of the pandemic (which determines the upper bound) and given the expectation about background mortality that is unaffected by the pandemic (which determines the lower bound). Indeed, if we fit the model to the post-pandemic data by estimating d_l and d_u jointly with η_0 and λ using the time series following the main pandemic waves, we find that disease outbreak probabilities for large outbreaks are reduced.

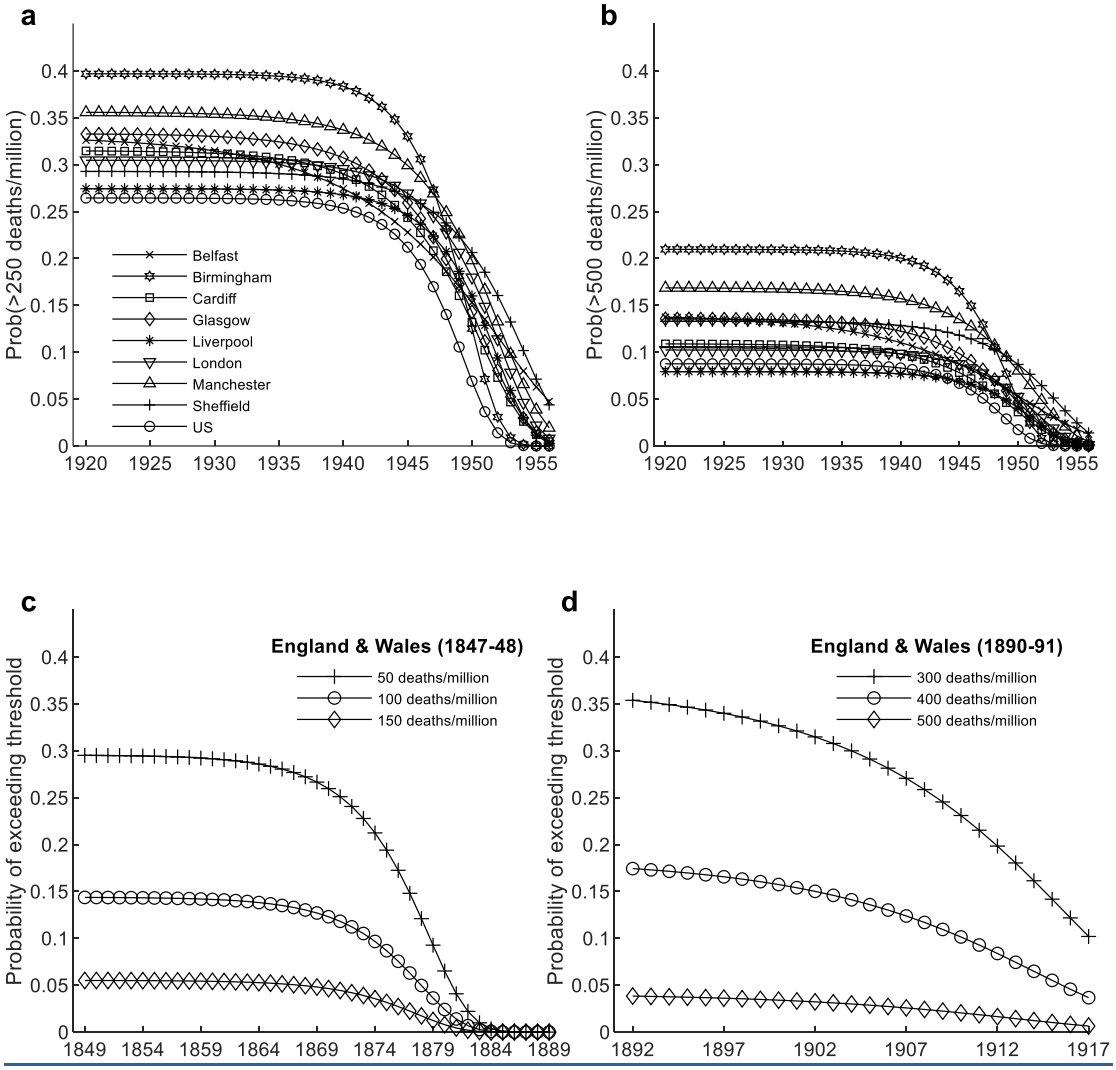

Figure A5: Outbreak risk following the relevant pandemic using the model with estimated bounds. (a-b) for the models fitted to the city data and the US following the 1918-19 pandemic, for thresholds of 500 and 1,000 per million; (c-d) for the models fitted to the England & Wales data following the 1847-48 pandemic (c) and the 1889-90 pandemic (d) for different thresholds.

One-parameter Weibull model

To further illustrate key points of the relevance of the Pareto distribution, we describe and fit a model with an alternative one-parameter distribution that allows for high probabilities for outcomes associated with the tail, the one-parameter Weibull-type distribution (12). In this case, mortality rates are drawn from:

$$d_t \sim W_t(w_t), \qquad (4)$$

where $w_t \in [0,1]$, noting that the tail contracts as w_t decreases. Assume that:

$$w_t = w_0 e^{-\lambda t}. \quad (5)$$

Conditional on the time process in (5), and thus conditional on the sequence $(w_t)_{t=0}^{N}$, d_t is independently distributed over time following (4). The likelihood is given by:

$$L(\lambda, w_0) = \prod_{t=0}^{N} \frac{log^3(w_0 e^{-\lambda t})}{log(w_0 e^{-\lambda t})-2} \bar{d}_t \left(\bar{d}_t + 1\right)\left(w_0 e^{-\lambda t}\right)^{\bar{d}_t},$$

for a sample of mortality rates $\left(\bar{d}_t\right)_{t=0}^{N}$. The results from this model, shown in Figure A6 also reveal that mortality risk remains high for a long period after the main pandemic waves, and that its dynamic pattern is similar across geographical units. However, the predicted probabilities for disease outbreaks are higher than those in Figure 4. This is an implication of the one-parameter Weibull form that delivers a fat tail by shifting the mass of the distribution away from lower numbers.[10] Moreover, disease outbreak risk inherits a rate of rapid decline from the exponential decay of w_t, the Weibull parameter that determines the thickness of the tail. This analysis demonstrates the importance of the property of the Pareto distribution that it can accommodate a fat tail with the mass of the distribution near the lower bound of outcomes. Alternative distributions that can deliver a concentration at lower mortality levels while also allowing for high probabilities associated with tail outcomes require more parameters to be specified (e.g. lognormal, Gaussian mixture) and require more assumptions regarding the dynamic transition. In particular, the model must specify the dynamic evolution of two or more parameters and a means to identify the specific combination of the dynamic processes of these parameters that characterises the evolution of tail probabilities and of mortality risk more generally. Data availability restricts these options. Being a one-parameter distribution conditional on the bounds for mortality rates, the bounded Pareto offers a transparent way to model the post-pandemic dynamic evolution of mortality and disease outbreak risk.

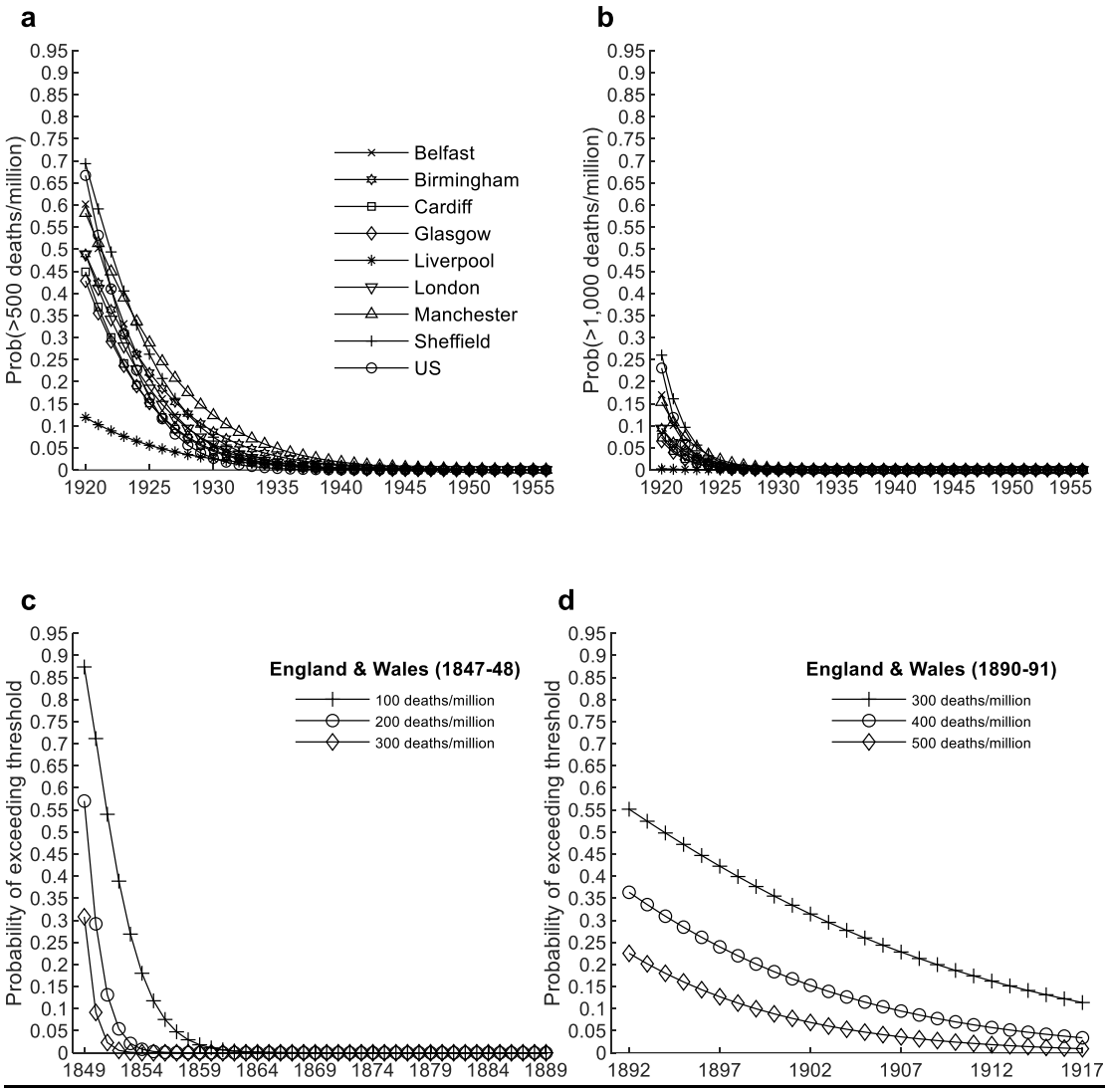

Figure A6: Outbreak risk following the relevant pandemic using the one-parameter Weibull model (i.e. assuming data for each year are drawn from a sequence of one-parameter Weibull distributions). (a-b) for the models fitted to the city data and the US following the 1918-19 pandemic, for thresholds of 500 and 1,000 per million; (c-d) for the models fitted to the England & Wales data following the 1847-48 pandemic (c) and the 1889-90 pandemic (d) for different thresholds.

Parameterisation of model of outbreaks following COVID-19

We assume that the parameters η_0 and λ that are relevant to a new pandemic are drawn from the same distribution from which the parameters in *Table* are drawn, and then perform a Monte Carlo analysis that provides a distribution of possible outcomes as a function of draws of η_0 and λ from that distribution, shown in Figure A7. We draw one million pairs of η_0 and λ from the implied joint density and summarise relevant percentiles of the generated distribution of predicted probabilities of mortality rates in Figure 5 in the main text.

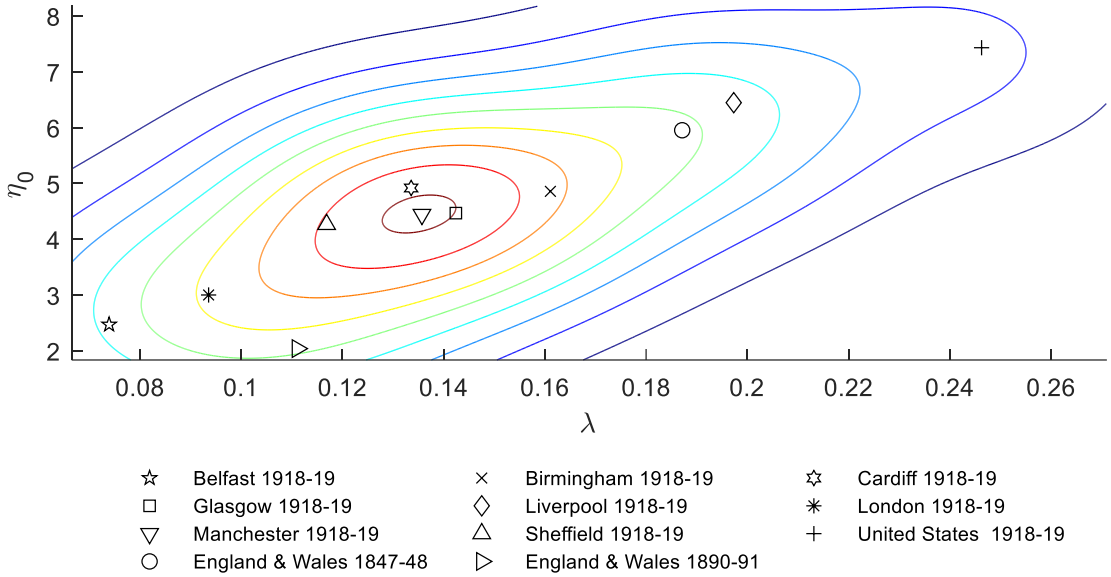

Figure A7: Distribution of η_0 and λ implied by the models fitted to previous pandemics. Estimates from Table B1 are shown with shapes. Contour lines represent smoothed kernel densities of combinations of η_0 and λ.

Monte Carlo Analysis

To conduct the analysis presented in Figure 2 in the main text and Figure B-1 in the SI, we proceed as follows. First, we select values for η_0, λ, d_l and d_u. To evaluate how our estimator behaves across a range of empirically relevant parameterisations, we select the values that are presented in Table B-1. Then, for each of these parameterisations, we simulate a set of 10,000 mortality rate time series of length 37. Finally, we estimate η_0 and λ for each of these simulated datasets using the approach described in Section B of this Supplementary Information. The output is then summarised in the form of Figures 2 and B-1.

References

1. Wellcome Trust, The Medical Officer of Health reports (2021) (August 18, 2021).
2. F. E. Linder, R. D. Grove, *Vital statistics rates in the United States, 1900-1940* (US Government Printing Office, 1943).
3. R. D. Grove, A. M. Hetzel, *Vital statistics rates in the United States, 1940-1960* (US Department of Health, Education, and Welfare, Public Health Service …, 1968).
4. Products - Vital Statistics of the US - Homepage (2015) (August 26, 2021).
5. C. Langford, The age pattern of mortality in the 1918-19 influenza pandemic: an attempted explanation based on data for England and Wales. *Medical History* **46**, 1–20 (2002).
6. H. Ritchie, *et al.*, Coronavirus Pandemic (COVID-19). *Published online at OurWorldInData.org* (2020) (August 18, 2021).
7. ONS, Population estimates - Office for National Statistics (2021) (August 18, 2021).
8. ONS, Influenza deaths in 2018, 2019 and 2020 - Office for National Statistics (2021) (August 18, 2021).
9. ONS, Population estimates for the UK, England and Wales, Scotland and Northern Ireland - Office for National Statistics (2019) (August 18, 2021).
10. M. Schroeder, S. Lazarakis, R. Mancy, K. Angelopoulos, “How do pandemics end? Two decades of recurrent outbreak risk following the main waves” https:/doi.org/10.21203/rs.3.rs-893004/v2 (October 14, 2021).
11. P. Cirillo, N. N. Taleb, Tail risk of contagious diseases. *Nature Physics 2020 16:6* **16**, 606–613 (2020).
12. A. Alexopoulos, One-Parameter Weibull-Type Distribution, Its Relative Entropy with Respect to Weibull and a Fractional Two-Parameter Exponential Distribution. *Stats* **2**, 34–54 (2019).